

Synthesis and Characterization of Ni-Doped ZnO Thin Films Prepared by Sol–Gel Spin-Coating Method

M. Ayachi^{a,b}, F. Ayad^a, A. Djelloul^{b,*}, L. Benharrat^b, and S. Anas^b

^a Université Mohamed Seddik Ben Yahia, Jijel, Algérie

^b Centre de Recherche en Technologie des Semi-Conducteurs pour l’Énergétique “CRTSE” 02 BdFrantz Fanon. BP 140, 7 Merveilles, Alger, Algérie

*e-mail: djelloulrtse@gmail.com

Received October 27, 2020; revised October 27, 2020; accepted December 28, 2020

Abstract—Ni-doped ZnO (ZnO:Ni) thin films were deposited onto glass substrate by sol–gel spin-coating method using zinc acetate dehydrate and nickel(II) chloride hexahydrate. The structural, morphological, and optical properties of ZnO:Ni thin films under various doping level of nickel were investigated using X-ray diffraction (XRD), ultraviolet–visible transmission spectra (UV–Vis), atomic force microscope (AFM), scanning electron microscopy (SEM) and Fourier transform infrared (FTIR) measurements. XRD patterns indicated that the deposited films had a crystalline hexagonal wurtzite structure with preferred orientation in the (0 0 2) plane when the grain size varied between 36.5 and 44.5 nm. All films were found to exhibit a good transparency in the visible range with the maximum transmittance of 95% and the optical band gap energies were found between 3.15 and 3.22 eV. The SEM morphology shows the non-doped and Ni-doped ZnO thin films are continuous, dense, and distributed over the entire area with good uniformity. All parameters procured for Ni:ZnO composite thin films propel the possibility of using composite thin films for transparent conducting electrode applications.

Keywords: ZnO:Ni, sol–gel spin-coating, structural, optical, morphological

DOI: 10.1134/S1063782621050043

1. INTRODUCTION

Zinc oxide (ZnO) is a broad-banded, direct-gap (3.37 eV) semiconductor compound belonging to the II–VI group of conductive transparent oxides (TCO) with n-type natural conductivity [1–3]. Currently, zinc oxide is one of the most studied materials due to its vast potential for thin-film technology applications. ZnO is a material whose use has now increased in several practical areas such as waveguides [4, 5] and piezoelectric transducers [6, 7], but also in various other areas such as gas sensors [8, 9], catalysts [10, 11], transparent conductive electrodes [12, 13], solar cells [14, 15], surface acoustic wave devices (SAW) [16, 17], and varistors [18, 19]. Zinc oxide (ZnO) is attracting a great attention due to its superior optical, electronic, and chemical properties [20], which could be applied to develop windows layers in photovoltaic solar cells [21] either intrinsic or doped with metals. The methods used for the elaboration of ZnO thin films are very different and numerous among the chemical and physical methods [22–31]. It is obvious that each method has its advantages and disadvantages and that the properties of the films depend on it enormously. Among different fabrication techniques, the sol–gel technique has been extensively used for film deposi-

tion [32, 33]. It offers advantages in producing thin, uniform, transparent, and multi-component oxide layers with many structures on various substrates [34, 35].

Diluted magnetic semiconductors (DMS) are semiconducting materials doped with 3d transition metals such as Co, Fe, Mn, or Ni that have attracted much interest in the last years because of their unique properties and potential application in spintronic, magnetoelectronic, and optoelectronic devices [36].

In this present work, non-doped and nickel-doped zinc oxide (ZnO) thin films have been prepared on glass substrates by spin-coating technique. We have investigated the influence of doping concentrations ranging from 0 to 6 at % on structural, optical, and morphological properties of ZnO thin films.

2. EXPERIMENTAL PROCEDURE

2.1. Preparation of Thin Film

After optimization of precursor solutions prepared by sol–gel routes, spin-coating technique was used for deposition of 3 layers for each thin film.

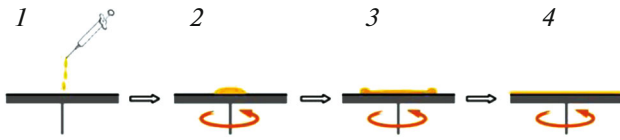


Fig. 1. A schematic of spin-coating process: 1—deposition, 2—acceleration, 3—flow domination, and 4—evaporation.

Highly-oriented non-doped and Ni-doped ZnO thin films were obtained according to the protocol presented on Fig. 1.

As shown in Fig. 1, the four basic stages in the spin-coating process are:

- (1) Deposition: deposition of solution onto the substrate.
- (2) Acceleration: spreading of solution from centre of substrate to the sides (spin-up).
- (3) Flow domination: gradual thinning of solution (spin-off).
- (4) Evaporation: gelation due to solvent evaporation.

Zinc acetate dihydrate and dopant were first dissolved in a methanol at room temperature. The dopant solution is taken at the atomic percentage of 0 to 6. The solutions were stirred at room temperature for 1 h to yield a clear and homogeneous solution. Prior to each deposition, the glass substrates were cleaned initially first by HCl then by ultrasonically in acetone and methanol for 15 min and finally washed with distilled water and dried.

The coating solutions with different dopants and concentrations were dropped onto a glass substrate under a rotation speed of 3000 rpm for 30 s by using a spin coater. After the deposition, the films were dried at 200°C for 10 min in the air (pre-heat treatment) to evaporate the solvent and remove organic residuals. The procedures from coating to drying were repeated many times. The films finally formed were annealed in air at 500°C for 1 h.

2.2. Characterization

The crystal phase and crystalline quality of prepared thin films were investigated by an X-ray diffractometer (BrukerD8) using $\text{CuK}\alpha$ radiation with a wavelength of 1.5406 Å in the range 25°–80°. The molecular structure was studied by using IR spectroscopy. The range of infrared radiation selected was 200–2000 cm^{-1} . The transmittance spectra were recorded by UV–Vis–NIR Lambda 950 spectrophotometer from PerkinElmer in the range of 200–800 nm. The surface morphology of the deposited thin film was studied using a SEM (FE1-XL30). All the measurements were carried out at room temperature.

3. RESULTS AND DISCUSSION

3.1. X-Ray Diffraction Analysis

Figure 2 shows the X-ray diffraction patterns of non-doped ZnO (Fig. 2a) and Ni-doped thin films (ZON) deposited with concentrations 2, 4, and 6% are presented on Figs. 2b, 2c, and 2d, respectively.

All XRD patterns of as prepared samples are compared to that of JCPDSN°36-1451 for ZnO with space group P63mc. The diffractograms of Figs. 2a–2d are assigned to the hexagonal wurtzite (WZ) crystalline phase of ZnO with preferred orientation in the (002) direction located around 34.40°. Moreover, the (002) diffraction peak intensities of Ni-doped ZnO films increased rapidly with nickel doping and were relatively higher than that ZnO non-doped thin film, which could either be due to the smaller difference in radius between Ni^{2+} ions (0.69 Å) and Zn^{2+} ions (0.74 Å) or that most of them have a strong c -axis orientation along (002) plane normal to the substrate [37]. However, the film deposited with 6 at % has the higher (002) intensity.

According to the XRD measurements, the thin films of Ni-doped ZnO are shown to adopt the preferred orientation with the c -axis (002) perpendicular to the substrate. The lattice spacing was calculated using the Bragg's formula [38]:

$$2d_{hkl} \sin \theta = n\lambda. \quad (1)$$

For hexagonal wurtzite structure, the lattice parameters a and c are related to d spacing and the Miller indices h , k , and l through the following equation [39]:

$$\frac{1}{d_{hkl}^2} = \frac{4}{3} \left[\frac{h^2 + hk + k^2}{a^2} \right] + \frac{l^2}{c^2}. \quad (2)$$

The average grain size of crystallite size was calculated by the Debye–Scherrer's equation as follows [40, 41]:

$$D = \frac{K\lambda}{\beta \cos \theta}, \quad (3)$$

where $(h k l)$ are Miller indices; d_{hkl} is the lattice spacing; θ is half of Bragg angle; λ is the wavelength of X-ray used (1.5406 Å); D is the grain size, β is the full width at half maximum (FWHM) of the diffraction peak.

The lattice strain ϵ was calculated from the relation [42–45]

$$\epsilon = \frac{\beta \cos \theta}{4}, \quad (4)$$

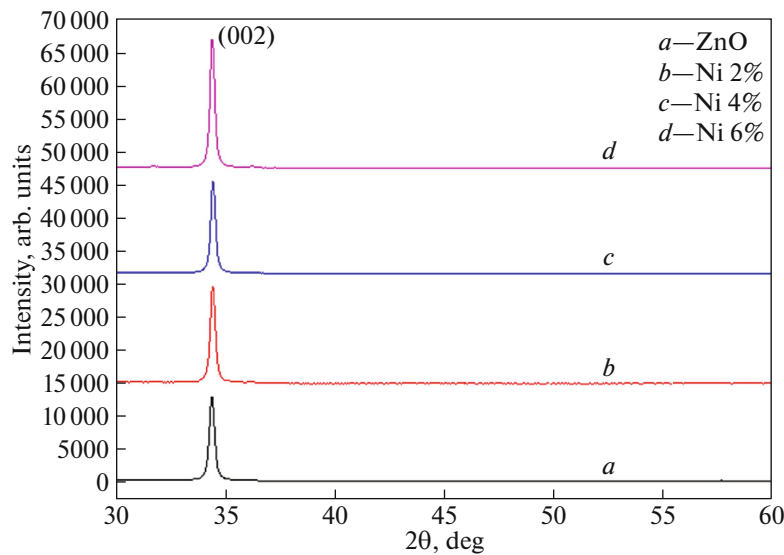


Fig. 2. X-ray diffraction spectra of the non-doped and Ni-doped ZnO thin film.

while the dislocation density δ was calculated by using the formula [46]

$$\delta = \frac{1}{D^2}. \quad (5)$$

The decrease in the FWHM of (002) crystal plane with doping concentration confirmed the increase in the crystallite size as shown in Table 1.

As shown in Table 1, with increasing Ni doping concentration, the lattice constant c decreases. Since the radius of Ni^{2+} (0.69 Å) is smaller than that of Zn^{2+} (0.74 Å), the variation of the c -axis lattice suggests that Ni substitutionally replaces Zn in the films [47, 48]. The average crystallite size of the NZO thin films varies from 36 to 43 nm and the strain values were found to be constantly decreasing with Ni-doping.

It is clear from XRD patterns of NZO samples that crystallinity quality increases as the concentration of Ni dopant is increasing and it is better than that of non-doped ZnO sample. M.S. Abdel-Wahab et al.

[49] also observed the similar trend with different doping concentrations. The change in the peak intensities can be attributed to the decrease in the defects of the stacking of thin films at different doping concentrations [50]. The absence of impurity peak related to Ni phase indicates successful incorporation of Ni in ZnO matrix, which is due to comparable ionic radius of Ni^{2+} (0.69 Å), and Zn^{2+} (0.74 Å) [51–58].

3.2. Optical Analysis

Figure 3 shows the optical transmittance spectrum of non-doped and Ni-doped ZnO thin films in the wavelength range from 200 to 800 nm. As can be seen from Fig. 3, all the films were highly transparent in the visible range (400–700 nm) with a transmittance of more than 90% even after Ni doping.

A sharp decrease in the transmittance is observed at about 378 nm, attributed to the band edge absorption. Also, no remarkable dependence of the measured

Table 1. The X-ray diffraction parameters value of non-doped and Ni-doped ZnO thin films: peak position 2θ , FWHM β , crystallite size D , Micro Strain ϵ , and dislocation density δ

Film	2θ , deg	FWHM, deg	β , deg	Crystallite size D , nm	Micro strain ϵ , %	$\delta \times 10^{14}$, lines/m ²	a , Å	c , Å	c/a	d , Å
ZnO	34.36	0.255	0.228	36.5	0.358	7.50	3.014	5.215	1.73	2.607
Ni 2%	34.40	0.234	0.207	40.2	0.328	6.18	3.011	5.210	1.73	2.605
Ni 4%	34.41	0.214	0.187	44.5	0.299	5.05	3.011	5.210	1.73	2.605
Ni 6%	34.38	0.219	0.192	43.3	0.307	5.33	3.012	5.213	1.73	2.606

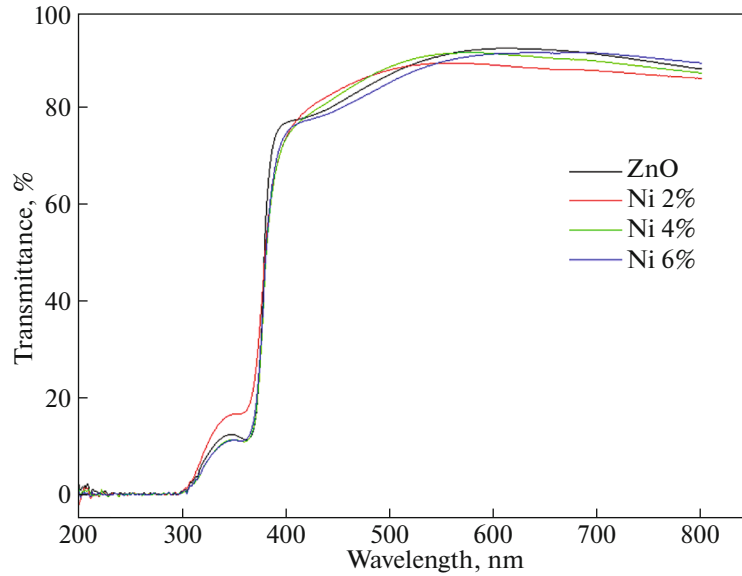


Fig. 3. Transmittance spectra of: (a) non-doped ZnO, (b) In-doped ZnO, and (c) Al-doped ZnO thin films deposited onto glass substrate.

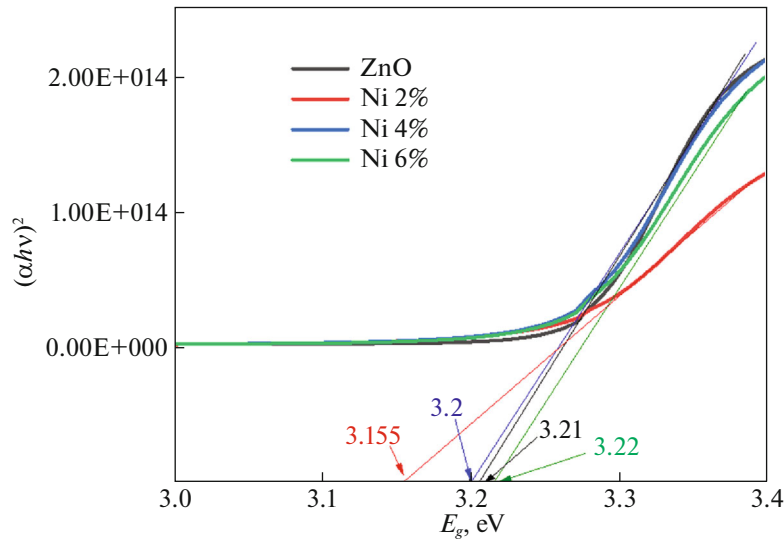


Fig. 4. Plots of $(\alpha h\nu)^2$ versus E_g for different Ni doping concentrations.

transmittance on the doping concentration of Ni in the studied range especially near the band edge was observed [59].

This value is reported by several authors; this enables ZnO films the character of transparent material and justify its application as front windows in optoelectronic devices [60, 61].

From transmittance measurements, the optical band gap can be estimated considering a direct-gap

semiconductor. The band gap (E_g) was calculated using the relation [62, 63]:

$$(\alpha h\nu)^2 = K(h\nu - E_g), \quad (6)$$

where h is Planck's constant, ν is the frequency of the incident radiation, K is a constant, and E_g is the band gap energy. The absorption coefficient α , which is a function of the photon energy $h\nu$, is calculated from

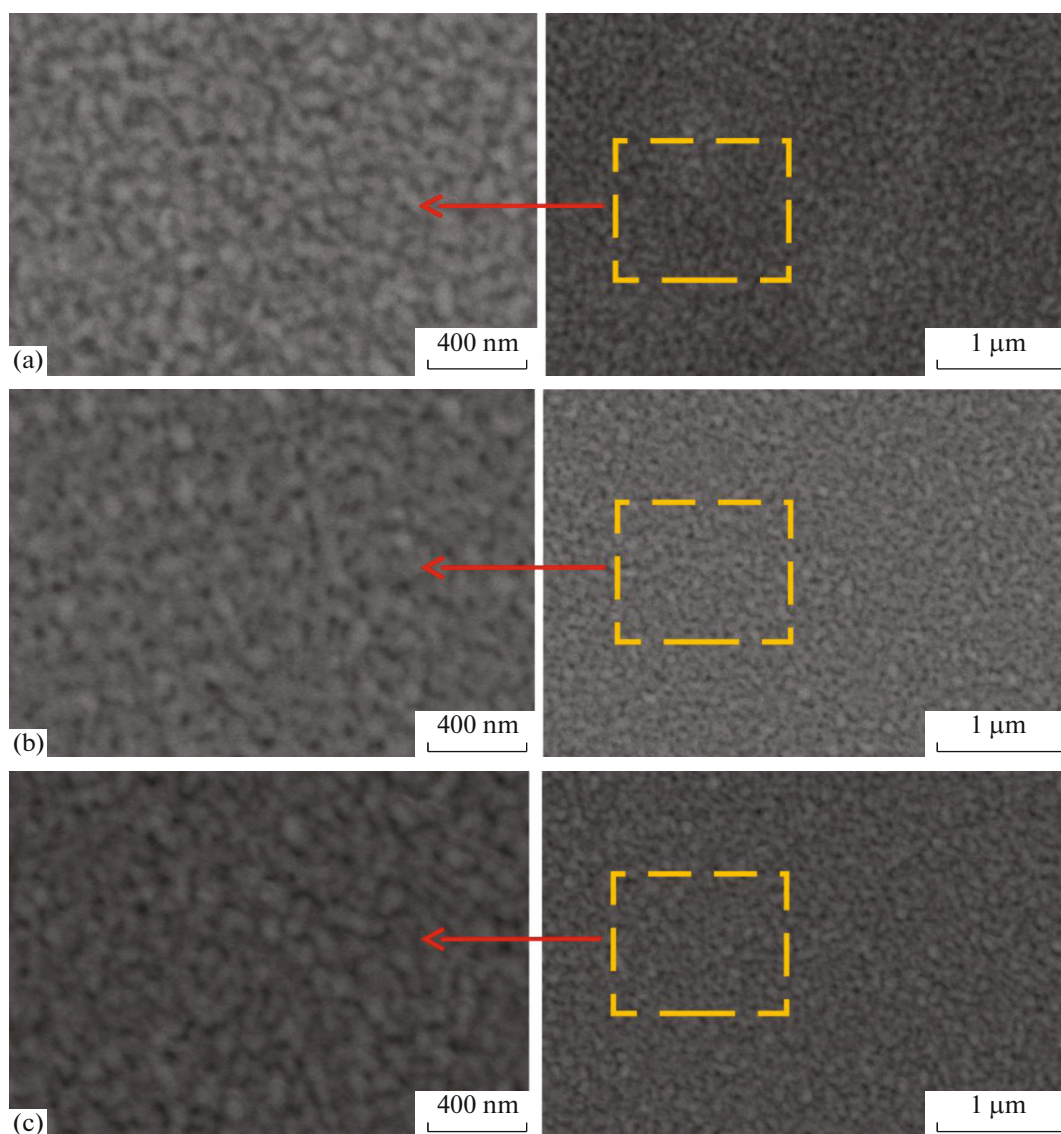


Fig. 5. SEM images of the films (a) ZnO pur, (b) ZnO–Ni 2% and (c) ZnO–Ni 6%.

the optical transmittance spectra results using equation [64]:

$$\alpha = \frac{-\ln(T)}{d}, \quad (7)$$

where d is the thickness of the film and T is the transmittance of the film.

The plots of $(\alpha h\nu)^2$ against E_g for the non-doped and Ni-doped ZnO thin films are shown in Fig. 4.

Band gap energy, determined by second-derivative spectrum [65], is obtained by extrapolating the linear portion of this graph to $(\alpha h\nu)^2 = 0$. As can be seen from Fig. 4, E_g (pure ZnO) is equal to 3.21 eV, E_g (2%) is equal to 3.155 eV, E_g (4%) is equal to 3.20 eV, and E_g (6%) is equal to 3.22 eV. It has been found that there is

no considerable effect of doping procedures. The estimated optical bands gaps coincide with those reported in literature and are slightly different from the bulk zinc oxide of 3.37 eV [66–70].

3.3. SEM Analysis

Figure 5a–5c shows the surface SEM micrographs of the non-doped and Ni-doped ZnO thin films.

All the films are dense, continuous, and distributed over the entire area with good uniformity. It is also clear that our layers have small uniform size grains in the form of nanoparticles with average diameter varying between 50 and 100 nm. However, the grain size as measured from the surface SEM images is higher than the values calculated from the XRD measurements,

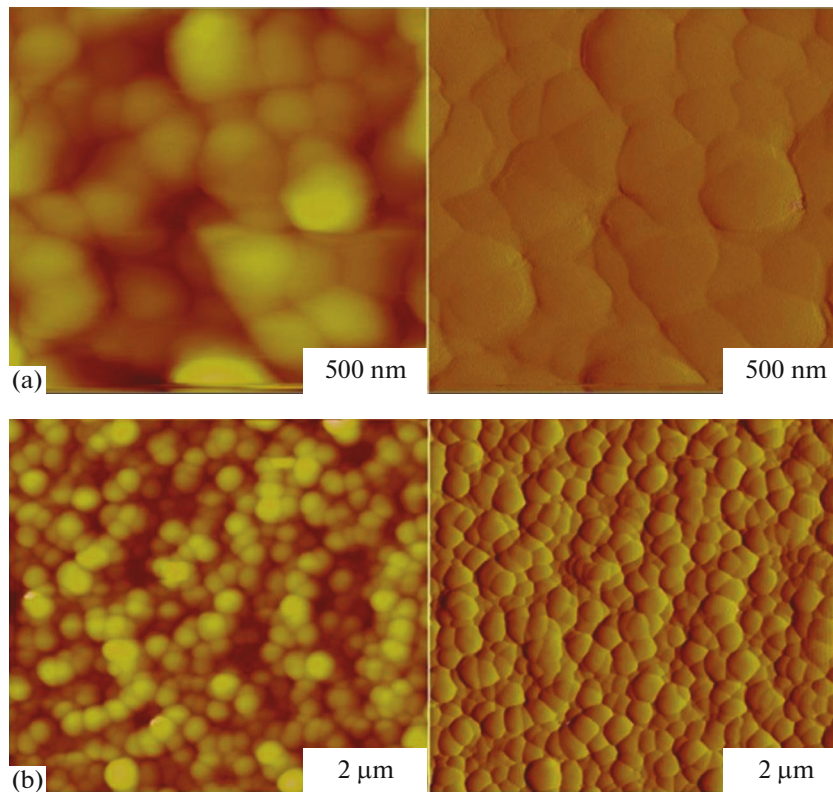


Fig. 6. AFM images of the films (a) ZnO pure, (b) Ni-doped ZnO thin films.

indicating that these grains are probably an aggregate of crystallites.

3.4. AFM Analysis

Morphological characterization of the non-doped and Ni-doped ZnO thin films were done by AFM analysis (Fig. 6).

Figures 6a and 6b shows the two-dimensional (2D) AFM images of the non-doped and Ni-doped films, respectively. The 2D images show that the films are uniform, dense, and distributed over the entire area with a rough surface. The shape of crystallites are the same, small crystallites form aggregates with average diameter varying between 50 and 100 nm. A few black patches also observed in the 2D AFM images of the non-doped and 2 at % Ni-doped thin films correspond to the presence of some voids on the film surface. Therefore, the Ni doping affects the surface topography of films and consequently can affect the optical properties. The average surface roughness and the average grain size decreases with Ni doping. This morphological change occurs due to incorporation of Ni ions into ZnO film matrix, resulting in variation in the lattice strain.

3.5. Fourier Transform Infrared Analysis

Fourier transform infrared (FTIR) spectroscopy supplements the information obtained from XRD and SEM. It is the combination of all data that helps us to understand, analyze, and refine more effectively the structure of films. FTIR spectroscopy is very useful tool for investigating vibrational properties of synthesized materials. The band positions and numbers of absorption peaks are depending on crystalline structure, chemical composition, and also on film morphology.

Figures 7a and 7b shows the FTIR spectra of pure and Ni-doped ZnO films, in the range of 4000–300 cm^{-1} [71, 72].

A band at 454 cm^{-1} is observed for each spectrum, which is attributed to the ZnO stretching vibrations [71, 73, 74]; these results are in good agreement with our XRD results and confirm the formation of ZnO [74]. The band around 2900 cm^{-1} is due to C–H (acetate) stretching [75]. The band at 1730 cm^{-1} is due to C=O stretching frequencies, and the band at 1424 cm^{-1} is the C–O stretch [71, 76].

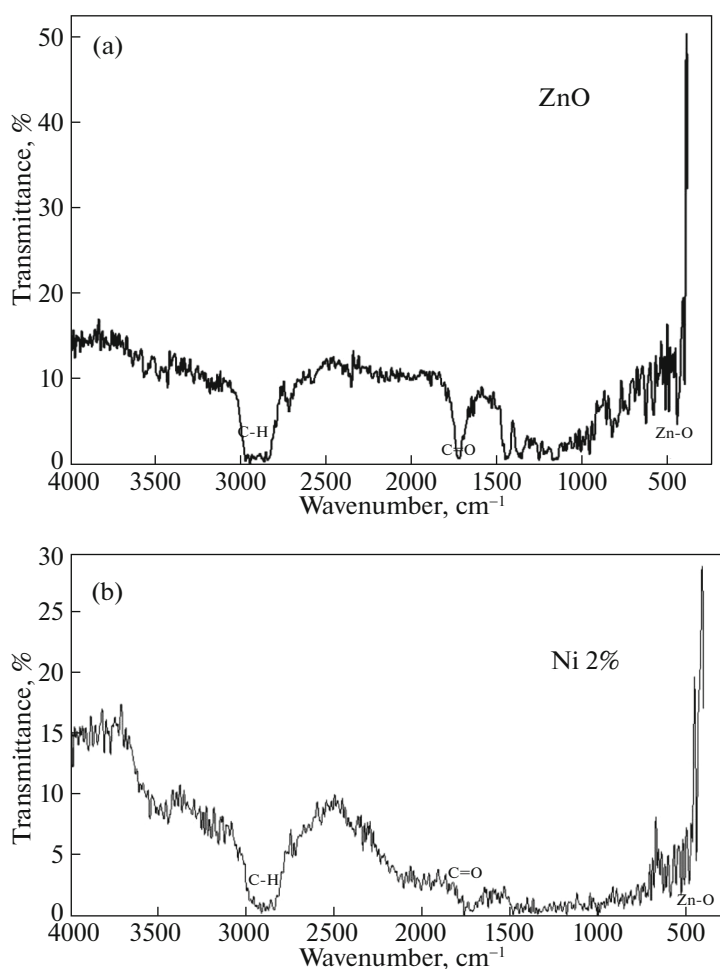


Fig. 7. FTIR spectrum and their peaks of pure and Ni-doped ZnO films.

4. CONCLUSIONS

The structural, optical, and morphological properties of non-doped ZnO and Ni-doped ZnO thin films deposited on glass substrates by spin-coating process were investigated. XRD analysis confirmed the hexagonal wurtzite crystalline phase of non-doped and Ni-doped zinc oxide thin films with preferred orientation in the (002) plane when the grain size varied between 36.5 and 44.5 nm. However, the film deposited with 6 at % has the higher (002) intensity. The optical measurement results confirmed that all the films were highly transparent in the visible range (400–700 nm) with a transmittance of more than 90% even after Ni doping. The optical gap of our ZnO samples was found between 3.15 and 3.22 eV. The morphological analysis confirmed that the shape of crystallites were the same, small crystallites formed aggregates with average diameter varying between 50 and 100 nm.

The obtained results indicate that the Ni-doped ZnO thin films elaborated by the spin-coating technique are promising candidate for optoelectronic

applications especially for electronic device applications.

ACKNOWLEDGMENTS

This work was supported by all members of Laboratory for the Study of Materials, University of Mohamed Seddik Ben Yahia of Jijel, Algeria.

CONFLICTS OF INTEREST

The authors declare that they have no conflict of interest.

REFERENCES

1. Z. N. Ng, K. Y. Chan, C. Y. Low, S. A. Kamaruddin, and M. Z. Sahdan, *Ceram. Int.* **41**, 254 (2015).
2. A. Bouaine, A. Bourebia, H. Guendouz, and Z. Riane, *Optik* **166**, 317 (2018).
3. D. Viet Vu, and D. Hai Le, C. Xuan Nguyen, and T. Quang Trinh, *J. Sol-Gel Sci. Technol.* **91**, 146 (2019).

4. S. Geburt, R. Röder, U. Kaiser, L. Chen, M.-H. Chu, J. Segura-Ruiz, G. Martínez-Criado, W. Heimbrod, and C. Ronning, *Phys. Status Solidi RRL* **7**, 886 (2013).
5. M. R. Maurya and V. Toutam, *Nanotechnol.* **30**, 085704 (2019).
6. K. Tao, H. Yi, L. Tang, J. Wu, P. Wang, N. Wang, L. Hu, Y. Fu, J. Miao, and H. Chang, *Surf. Coat. Technol.* **359**, 289 (2019).
7. J. Guo, B. Legum, B. Anasori, K. Wang, P. Lelyukh, Y. Gogotsi, and C. A. Randall, *Adv. Mater.* **30**, 1801846 (2018).
8. S. D. Shinde, V. B. Gaikwad, G. E. Patil, D. D. Kajale, and G. H. Jain, *Int. J. Nanopart.* **5**, 126 (2012).
9. W. Wang, H. Huang, Z. Li, H. Zhang, Y. Wang, W. Zheng, and C. Wang, *J. Am. Ceram. Soc.* **91**, 3817 (2008).
10. S. Polarz, J. Strunk, V. Ischenko, M. W. E. van den Berg, O. Hinrichsen, M. Muhler, and M. Driess, *Angew. Chem. Int. Ed.* **45**, 2965 (2006).
11. Won Il Park, D.-W. Kim, Sug Woo Jung, and G.-C. Yi, *Int. J. Nanotechnol.* **3**, 372 (2006).
12. D. Chen, J. Liang, C. Liu, G. Saldanha, F. Zhao, K. Tong, J. Liu, and Q. Pei, *Adv. Funct. Mater.* **25**, 7512 (2015).
13. S. Ghosh and S. Bhaktha, *Nanotechnology* **29**, 225202 (2018).
14. R. Azmi, W. T. Hadmojo, S. Sinaga, C. L. Lee, S. C. Yoon, I. H. Jung, and S. Y. Jang, *Adv. Energy Mater.* **8**, 1701683 (2017).
15. J. Choi, Y. Kim, J. W. Jo, J. Kim, B. Sun, G. Walters, F. P. García de Arquer, R. Quintero-Bermudez, Y. Li, C. S. Tan, L. N. Quan, A. P. T. Kam, S. Hoogland, Z. Lu, O. Voznyy, and E. H. Sargent, *Adv. Mater.* **29**, 1702350 (2017).
16. Y.-F. Chiang, C.-C. Sung, and R. Ro, *Appl. Phys. Lett.* **96**, 154104 (2010).
17. X. He, H. Guo, J. Chen, W. Wang, W. Xuan, Y. Xu, and J. Luo, *Appl. Phys. Lett.* **104**, 213504 (2014).
18. W. Long, J. Hu, J. Liu, J. He, and R. Zong, *J. Am. Ceram. Soc.* **93**, 2441 (2010).
19. J. Cai, Y.-H. Lin, M. Li, C.-W. Nan, J. He, and F. Yuan, *J. Am. Ceram. Soc.* **90**, 291 (2007).
20. Z. C. Feng, *Handbook of Zinc Oxide and Related Materials*, Vol. 1: *Materials* (Taylor and Francis, Boca Raton, 2013).
21. A. Djelloul, Y. Larbah, M. Adnane, B. Labdelli, M. I. Ziane, A. Manseri, and A. Messaoud, *J. Nano-Electron. Phys.* **10**, 02036 (2018).
22. V. Sharma, P. Kumar, J. Shrivastava, A. Solanki, V. R. Satsangi, S. Dass, and R. Shrivastav, *Int. J. Hydrogen Energy* **36**, 4280 (2011).
23. M. Karunakaran, R. Chandramohan, S. Balamurali, S. Gomathi, K. Kabila, and T. Mahalingam, *Int. J. Thin Film Sci. Tech.* **3**, 61 (2014).
24. S. Yilmaz, E. McGlynn, E. Bacaksız, J. Cullen, and R. K. Chellappan, *Chem. Phys. Lett.* **525–526**, 72 (2012).
25. J. P. Mathew, G. Varghese, and J. Mathew, *Sop. Trans. Appl. Phys.* **1**, 27 (2014).
26. Prerna, S. Arya, A. Sharma, B. Singh, A. Tomar, S. Singh, and R. Sharma, *Integr. Ferroelectr.* **205**, 1 (2020).
27. S. H. Basri, M. A. M. Sarjidan, and W. H. Abd Majid, *Adv. Mater. Res.* **895**, 250 (2014).
28. M. Sudha, S. Radha, S. Kirubaveni, R. Kiruthika, R. Govindaraj, and N. Santhosh, *Solid State Sci.* **78**, 30 (2018).
29. Y. J. Zeng, Z. Z. Ye, W. Z. Xu, B. Liu, Y. Che, L. P. Zhu, and B. H. Zhao, *Mater. Lett.* **61**, 41 (2007).
30. X. Liu, F. Lin, L. Sun, W. Cheng, X. Ma, and W. Shia, *Appl. Phys. Lett.* **88**, 062508 (2006).
31. W. Mista, J. Ziaja, and A. Gubanski, *Vacuum* **74**, 293 (2004).
32. A. Yildiz, B. Kayhan, B. Yurduguzel, A. P. Rambu, F. Iacomi, and S. Simon, *J. Mater. Sci. Mater. Electron.* **22**, 1473 (2011).
33. A. S. Ismail, M. H. Mamat, M. F. Malek, S. A. Saidi, M. M. Yusoff, R. Mohamed, N. D. Md Sin, A. B. Suriani, and M. Rusop, *AIP Conf. Proc.* **1963**, 020029 (2018).
34. G. Vijayaprasath, R. Murugan, G. Ravi, T. Mahalingam, and Y. Hayakawa, *Appl. Surf. Sci.* **313**, 870 (2014).
35. P. M. Tkachuk, A. I. Savchuk, I. D. Stolyarchuk, G. I. Kleto, S. A. Savchuk, and V. I. Tkachuk, in *Proceedings of the 11th International Conference on Correlation Optics*, Proc. SPIE **9066**, 906616 (2013).
36. X. Zhong, R. Xie, Y. Zhang, T. Basche, and W. Knoll, *Chem. Mater.* **17**, 4038 (2005).
37. S. Abed, M. S. Aida, K. Bouchouit, A. Arbaoui, K. Iliopoulos, and B. Sahraoui, *Opt. Mater.* **33**, 968 (2011).
38. C. Zegadi, A. Abderrahmane, A. Djelloul, S. Hamzaoui, M. Adnane, D. Chaumont, and K. Abdelkebir, *Int. Rev. Phys.* **9**, 39 (2015).
39. T. Prasada Rao and M. C. Santhosh Kumar, *Appl. Surf. Sci.* **255**, 4579 (2009).
40. A. Djelloul, M. Adnane, Y. Larbah, T. Sahraoui, C. Zegadi, A. Maha, and B. Rahal, *J. Nano-Electron. Phys.* **7**, 04045 (2015).
41. Y. Larbah, M. Adnane, and T. Sahraoui, *Mater. Sci.-Poland* **33**, 491 (2015).
42. T. S. Reddy and M. S. Kumar, *RSC Adv.* **6**, 95680 (2016).
43. M. Shkir, M. Kilany, and I. S. Yahia, *Ceram. Int.* **43**, 14923 (2017).
44. M. Shkir, M. Arif, V. Ganesh, M. A. Manthrammel, A. Singh, I. S. Yahia, S. R. Maidur, P. S. Patil, and S. AlFaify, *J. Mater. Res.* **33**, 3880 (2018).
45. S. Mohd, Z. R. Khan, M. S. Hamdy, H. Algarni, and S. AlFaify, *Mater. Res. Express* **5**, 095032 (2018).
46. M. Azizar Rahman and M. K. R. Khan, *Mater. Sci. Semicond. Process.* **24**, 26 (2014).
47. D.-L. Hou, R.-B. Zhao, Y.-Y. Wei, C.-M. Zhen, C.-F. Pan, and G.-D. Tang, *Curr. Appl. Phys.* **10**, 124 (2010).
48. A. A. Aboud, M. Shaban, and N. Revaprasadu, *RSC Adv.* **9**, 7729 (2019).
49. M. S. Abdel-Wahab, A. Jilani, I. S. Yahia, and A. A. Al-Ghamdi, *Superlatt. Microstruct.* **94**, 108 (2016).

50. S. H. Basri, M. A. Mohd Sarjidan, and W. H. Abd Majid, *Adv. Mater. Res.* **895**, 250 (2014).
51. D. Iskenderoğlu and H. Güney, *Ceram. Int.* **43**, 16593 (2017).
52. V. Sharma, P. Kumar, J. Shrivastava, A. Solanki, V. R. Satsangi, S. Dass, and R. Shrivastav, *Int. J. Hydrogen Energy* **36**, 4280 (2011).
53. M. Karunakaran, R. Chandramohan, S. Balamurali, S. Gomathi, K. Kabila, and T. Mahalingam, *Int. J. Thin Film Sci. Technol.* **3**, 61 (2014).
54. M. El-Hilo, A. A. Dakhel, and A. Y. Ali-Mohamed, *J. Magn. Magn. Mater.* **321**, 2279 (2009).
55. L. Herissi, L. Hadjeris, M. S. Aida, S. Azizi, A. Hafdalalah, and A. Ferdi, *Nano Hybrids. Compos.* **27**, 21 (2019).
56. D.-L. Hou, R.-B. Zhao, Y.-Y. Wei, C.-M. Zhen, C.-F. Pan, and G.-D. Tang, *Curr. Appl. Phys.* **10**, 124 (2010).
57. C. M. Muiva, T. S. Sathiaraj, and K. Maabong, *Ceram. Int.* **37**, 555 (2011).
58. A. K. Rana, P. Bankar, Y. Kumar, M. A. More, D. J. Late, and P. M. Shirage, *RSC Adv.* **6**, 104318 (2016).
59. A. A. M. Farag, M. Cavas, F. Yakuphanoglu, and F. M. Amanullah, *J. Alloys Compd.* **509**, 7900 (2011).
60. M. Y. Ali, M. K. R. Khan, A. M. M. Tanveer Karim, M. Mozibur Rahman, and M. Kamruzzaman, *Heliyon* **6**, e03588 (2020).
61. S. Thakur, J. Kumar, J. Sharma, N. Sharma, and P. Kumar, *J. Optoelectron. Adv. Mater.* **15**, 989 (2013).
62. B. Subramanian, C. Sanjeeviraja, and M. Jayachandran, *J. Cryst. Growth* **234**, 421 (2002).
63. A. Djelloul, M. Adnane, Y. Larbah, M. Zerdali, C. Zegadi, and A. Messaoud, *J. Nano- Electron. Phys.* **8**, 02005 (2016).
64. A. Djelloul, M. Adnane, Y. Larbah, and S. Hamzaoui, *J. Opt. Adv. Mater.* **18**, 136 (2016).
65. D. Djouadi, A. Chelouche, A. Aksas, and M. Sebais, *Phys. Proc.* **2**, 701 (2009).
66. H. A. Dehkordi, A. Mokhtari, K. Dastafkan, and V. Soleimanian, *J. Electron. Mater.* **48**, 1258 (2019).
67. C.-Q. Luo, C.-C. F. Ling, M. A. Rahman, M. Phillips, C. Ton-That, C. Liao, K. Shih, J. Lin, H. W. Tam, A. B. Djuri, and S.-P. Wang, *Appl. Surf. Sci.* **483**, 1129 (2019).
68. A. C. Gandhi, C.-H. Liao, W.-L. Yeh, and Y.-L. Huang, *RSC Adv.* **9**, 2180 (2019).
69. A. M. M. T. Karim, M. M. Rahman, M. Shahjahan, and M. K. R. Khan, *Mater. Res. Express* **2**, 036402 (2015).
70. A. M. M. T. Karim, M. K. R. Khan, and M. M. Rahman, *Mater. Sci. Semicond. Process.* **41**, 184 (2016).
71. P. Mitra and S. Mondal, *Prog. Theor. Appl. Phys.* **1**, 17 (2013).
72. A. Djelloul, M.-S. Aida, and J. Bougdira, *J. Lumin.* **130**, 2113 (2010).
73. T. Ivanova, A. Harizanova, T. Koutzarova, and B. Vertruyen, *Mater Lett.* **64**, 1147 (2010).
74. S. Kumar, R. Kumar, and D. P. Singh, *Appl. Surf. Sci.* **255**, 8014 (2009).
75. S. Senthilkumaar, K. Rajendran, S. Banerjee, T. K. Chini, and V. Sengodan, *Mater. Sci. Semicond. Process.* **11**, 6 (2008).
76. M. N. Kamalasanan and S. Chandra, *Thin Solid Films* **288**, 112 (1996).